Rapid adaptive evolution of microbial thermal performance curves

Megan H. Liu[1,*], Ze-Yi Han[1], Yaning Yuan[1], Katrina DeWitt[1], Daniel J. Wieczynski[1], Kathryn M. Yammine[2], Andrea Yammine[1], Rebecca Zufall[3], Adam Siepielski[4], Douglas Chalker[5], Masayuki Onishi[1], Fabio A. Machado[6], Jean P. Gibert[1,*]

[1]Department of Biology, Duke University, Durham, NC, 27708, USA
[2]Department of Chemistry, Massachusetts Institute of Technology, Cambridge, MA, 02139, USA
[3]Department of Biology and Biochemistry, University of Houston, Houston, TX 77204, USA
[4]Department of Biological Sciences, University of Arkansas, Fayetteville, AR, USA
[5]Department of Biology, Washington University, Saint Louis, MI, USA
[6]Department of Integrative Biology, Oklahoma State University, Stillwater, OK, USA

To whom correspondence should be addressed: mhliu58@gmail.com, jean.gibert@duke.edu

KEYWORDS
Thermal Adaptation, Thermal Performance Curve Heritability, Climate Change, Quantitative Genetics

DATA AND CODE AVAILABILITY:
Data and code will be archived upon publication.

ACKNOWLEDGMENTS
We are grateful to Enzo Bruscato and Heather Raslan for their data collection support. We are indebted to Samraat Pawar for his thoughtful feedback. AMS was supported by NSF DEB award 2306183. DLC acknowledges grant support for the Tetrahymena Stock Center by NIH project # 2P40OD010964 and additional support from NSF award # MCB 1947526. JPG acknowledges generous support from DOE BER DE-SC0020362 (which also supported MHL, AY, and DJW), NSF DEB award number 2224819, NSF CAREER award number 2337107, and a Simons Foundation Early Career Fellowship in Microbial Ecology and Evolution LS-ECIAMEE-00001588 (which also supported MHL and AY).

ABSTRACT

Microbial respiration alone releases massive amounts of Carbon (C) into the atmosphere each year, greatly impacting the global C cycle that fuels climate change. Larger microbial population growth often leads to larger standing biomass, which in turns leads to higher respiration. How rising temperatures might influence microbial population growth, however, depends on how microbial thermal performance curves (TPCs) governing this growth may adapt in novel environments. This thermal adaptation will in turn depend on there being heritable genetic variation in TPCs for selection to act upon. While intraspecific variation in TPCs is traditionally viewed as being mostly environmental (E, or plastic) as a single individual can have an entire TPC, our study uncovers substantial heritable genetic variation (G) and Gene-by-Environment interactions (GxE) in the TPC of a widely distributed ciliate microbe. G results in predictable evolutionary responses to temperature-dependent selection that ultimately shape TPC adaptation in a warming world. Through mathematical modeling and experimental evolution assays we also show that TPC GxE leads to predictable temperature-dependent shifts in population genetic makeup that constrains the potential for future adaptation to warming. That is, adaptive evolution can select for decreased genetic variation which subsequently lowers the evolutionary potential of microbial TPCs. Our study reveals how temperature-dependent adaptive evolution shapes microbial population growth, a linchpin of global ecosystem function, amidst accelerating climate warming.

INTRODUCTION

Microbes play a central role regulating the global carbon (C) cycle that controls climate change (Davidson & Janssens, 2006; Falkowski et al., 2008; Trumbore, 2006). Indeed, soil microbial respiration releases ~94Pg of C into the atmosphere every year (Bond-Lamberty, 2018; Stell et al., 2021; Xu & Shang, 2016) and microalgae provide the bulk of marine C fixation globally (30-50 Pg of C/yr) (Arrigo, 2005; Falkowski, 1994; Litchman et al., 2015). Global warming is expected to alter these microbial processes (Intergovernmental Panel on Climate Change (IPCC), 2023), but anticipating these effects requires a deeper understanding of the biotic and abiotic factors influencing microbial respiration in a warming world (Barton et al., 2020; Rocca et al., 2022; Wieczynski et al., 2023). One such factor is microbial population growth, which influences total standing biomass, and hence, total microbial respiration (Brown et al., 2004; DeLong et al., 2017; Gillooly et al., 2001; Savage et al., 2004).

To understand and anticipate the effects of global warming, we need to characterize the evolutionary processes that shape the microbial Thermal Performance Curves responsible for determining microbial population growth under novel climates. Microbial thermal performance curves are often measured as change in maximum (intrinsic) population growth rates (denoted *r*, the difference between per capita birth and death rates) across temperatures ('r-TPCs' henceforth, Fig 1). They thus determine how a species population growth rate will change in response to temperature changes. Controlled by temperature-dependent metabolic rates, r-TPCs are typically unimodal: increasing temperatures lead to rising metabolic rates and population growth until an 'optimal' temperature (T_{opt}) is reached (Fig 1a). Beyond T_{opt}, elevated metabolic costs slow down or impede growth (Amarasekare & Savage, 2012; Brown et al., 2004; Rebolledo et al., 2020; Sinclair et al., 2016), Fig 1a). While unimodality is the norm, r-TPC

shape often varies across species (Kellermann et al., 2019) due to differences in microbial traits (Wieczynski et al., 2021) and genetic expression between closely related species (Jacob & Legrand, 2021). Ultimately, however, differences in r-TPC shape are attributed to divergent evolutionary trajectories across species and environmental conditions (Angilletta, 2009; Kontopoulos et al., 2020; Malusare et al., 2023).

Despite these recent findings, predicting how r-TPCs might adapt to future warming climates remains an unsolved but central challenge, as r-TPC adaptation underpins a species' ability to cope with environmental change. Thermal adaptation hinges on the evolution of intraspecific genetic variation through mutation (Kirkpatrick & Peischl, 2013) and selection favoring genetic variants that perform better in novel environments (Barrett & Schluter, 2008; Franks et al., 2007). Characterizing this intraspecific variation in r-TPCs is therefore central to understanding and predicting how rising temperatures will influence microbial growth in novel climates (Kling et al., 2023). Most intraspecific variation in microbial r-TPCs is likely coming from plastic variation in r across temperatures —known as environmental variation (E)—as a single clonal line or individual can have an entire TPC. However, additive genetic variation (G) in r-TPCs—upon which selection acts (Frankham, 2005)—is also likely (Kling et al., 2023; Liu et al., 2020; Singleton et al., 2021), and can ultimately decide how thermal adaptation occurs. Last, selection may act on plasticity itself, whenever there are fitness consequences associated with genetic variation in environmental responses (or G × E interactions, (Hoffmann & Sgrò, 2011)). In this case, plasticity can help drive adaptive evolution (Ghalambor et al., 2007; Kling et al., 2023). Quantifying and characterizing the genetic variation in microbial r-TPCs, as well as how that variation influences r-TPCs response to selection in novel environments, is thus paramount.

In this study we ask: 1) What is the extent of heritable G and G × E variation in r-TPCs? 2) What are the evolutionary consequences of G in r-TPCs under warming, and does G influence r-TPC shape (henceforth 'shape parameters', Fig 1b) in response to selection across temperatures? Lastly, 3) What are the evolutionary consequences of G × E in r-TPCs under warming? We address these questions in a globally important ciliate protist species—i.e., unicellular Eukaryotes that dominate oceanic biomass (Bar-On & Milo, 2019), hold twice the biomass of the entire Animal Kingdom (Bar-On et al., 2018), rank third in terrestrial biomass (Bar-On et al., 2018), and underpin global ecosystem functioning (Geisen et al., 2018; Hu et al., 2021; Nguyen et al., 2020; Xiong et al., 2020).

RESULTS

r-TPC variation and heritability

Intraspecific variation in r-TPCs can be quantified using classic tools from quantitative genetics where r-TPCs are interpreted as the reaction norm of *r* across temperatures (Fig 1c-e). Under this quantitative genetics framework, purely plastic variation (E) should result in similar r-TPCs across genotypes (Fig 1c), additive genetic variation (G) should result in parallel r-TPCs among genotypes (Fig 1d), and G × E interactions should result in non-parallel r-TPCs among genotypes (Fig 1e). To quantify these different sources of r-TPCs variation, we leveraged a collection of 22 unique genotypes of the protist *Tetrahymena thermophila* from the Cornell *Tetrahymena* Stock Center (see Methods, Appendix S1). We quantified r-TPCs using standard population growth assays across seven temperatures (13, 19, 22, 25, 30, 32, and 38ºC) replicated six times each (see Methods). These temperatures span below and above the incubation

133 temperature of 22ºC and the average summer temperature (~23ºC, (NOAA)) of the species'
134 native range (US Northeast, Zufall et al., 2013).

135 All r-TPCs showed strong unimodal temperature effects on *r* within genotypes (R^2=
136 0.784, Fig 2a). r-TPCs showed significant variability in shape across genotypes (F= 163.65, $p \leq$
137 0.001, $D_f = 21$, Generalized Eta-Squared (GES, =effect sizes) = 0.832, Fig 2a) and significant G
138 × E interactions (F=29.7, $p \leq 0.001$, $D_f = 122$, GES = 0.840, Fig 2a). Environmental variation (E)
139 accounted for 71.7% of all observed variation in r-TPCs; genetic variation (G) explained 6.1% of
140 all variation; Gene-by-Environment interactions (G × E) explained 11.7% of all variation, and
141 10.5% was residual variation (Fig 2b). These patterns are in line with what is expected for life
142 history traits (Hoffmann & Sgrò, 2011). After accounting for experimental error in the form of
143 inter-treatment and replicate variability (see calculation of broad-sense heritability, Methods), r-
144 TPCs were strongly heritable ($H^2_{standard}$=0.76, H^2_{cullis}=0.95, H^2_{piepho}=0.91).
145
146 *Consequences of G: selection and evolvability of r-TPC shape parameters*
147 In the presence of heritable genetic variation (G), r-TPCs shape may evolve under
148 selection. To understand this phenomenon, we quantified four 'shape' parameters controlling the
149 rising portion of the TPC, i.e., the 'operational temperature range' (DeLong et al., 2017; Smith et
150 al., 2021), Fig 1b). We focus on the rising portion because temperatures within this range often
151 control ecological responses to warming for *T. thermophila* in its native range (Deutsch et al.,
152 2008; Schoolfield et al., 1981; Schulte et al., 2011). To do so, we fitted a Sharpe-Schoolfield
153 model (Schoolfield et al., 1981) on r-TPC data (Fig 1a, b, see Methods) and determined the
154 critical minimal temperature (CT_{min}, Fig 1b), the 'activation energy' (E_a, Fig 1b), the maximum
155 population growth (r_{peak}, Fig 1b), and the temperature of maximal growth (T_{opt}, Fig 1a, b, see

Methods). We then estimated the intraspecific variation within each parameter, and the form of selection acting on them with and without taking genetic covariances into account (see Methods). Genetic covariances among shape parameters can lead to joint parameter evolutionary responses irrespective of direct selection acting on a given shape parameter, or even preclude parameter evolution altogether (Hansen & Houle, 2008). To estimate the predicted evolutionary change of each parameter under different temperature scenarios, we used a modified G-matrix approach that jointly estimates the genetic variance-covariance among shape parameters and the predicted parameter change ($\mathbf{\Delta z}$) across temperatures using a modified Price equation (see Methods, Stinchcombe et al., 2014). This approach allowed us to estimate the selection gradient ($\mathbf{\beta}$) acting directly on the shape parameters while controlling for effects of environmentally induced trait-fitness covariances (see Methods), which provides a better estimate of selection on the traits of interest than the standard multivariate breeder's equation (Lande, 1979; Lande & Arnold, 1983; Stinchcombe et al., 2014).

Without accounting for genetic associations, selection operated differentially across shape parameters and was temperature dependent: r_{peak} was under negative directional selection at low temperatures (<20°C, Fig 3a, Appendix S1), under weakly positive or no selection at intermediate temperatures (between 20 and 30°C, Fig 3a, Appendix S1), and under strong positive directional selection in high temperatures. Parameter E_a followed a similar pattern (Fig 3b, Appendix S2). However, CT_{min} was found to be under negative selection at low/intermediate temperatures (Fig 3c, Appendix S3) but no selection at high temperatures (Fig 3c, Appendix S3). Lastly, T_{opt} was under no selection at low temperatures but under weak then strong stabilizing selection at intermediate and high temperatures, respectively (Fig 3d, Appendix S4).

We found clear positive genetic covariances between shape parameters, specifically, between r_{peak} and E_a, CT_{min} and E_a, and CT_{min} and T_{opt} (Fig 3e). Accounting for these genetic associations, we again found differences in selection across shape parameters whose magnitude and direction also shifted with temperature (Fig 3f), resulting in predicted temperature-dependent shifts in parameter responses (Fig 3g). Specifically, our multivariate selection analysis suggested that selection would favor higher r_{peak} and E_a at high temperatures (Fig 3f), however, predicted responses in both cases should result in low values at low temperatures and high values at high temperatures (Fig 3g), consistent with our univariate analysis. Similarities of the adaptive landscapes for both shape parameters are mostly given by their strong positive genetic correlation (Fig 3e), and their response at low temperatures are likely driven by genetic correlations with CT_{min}. Indeed, we identified mostly negative selection on CT_{min} (except at high temperatures, where no significant selection was found) and no selection for T_{opt}, also in accordance with the univariate analysis (Fig 3f). Overall, the evolutionary responses followed predicted trajectories from the estimates of selection closely (Fig 3f-g), suggesting little effect of potential antagonistic selection on genetic constraints in r-TPC shape.

Consequences of G × E: differential sorting of standing genetic variation across temperatures

In the presence of G × E—where genotypes express different r-TPCs at different temperatures—small differences in TPCs can lead to differential growth among genotypes across temperatures, leading to clonal sorting and swift changes in population genetic makeup, i.e., evolution (Fig 4a, b). We tested this form of temperature-mediated rapid evolution induced by r-TPC GxE through an experimental evolution assay: we competed two fluorescently tagged genotypes (Fig 4c, AXS and CU4106, see Methods) with different r-TPCs (Fig 4d), hence

differing in relative fitness across temperatures (Fig 4d, inset). We observed significant temperature-dependent clonal sorting (Fig 4e), which matched theoretical predictions from a model of genetic evolution (Fig 4f). The model predicts genetic frequencies in a mixture population using parameters taken from each genotype's r-TPC, as well as patterns of relative fitness (Fig 4d) between the genotypes from r-TPC data (see Methods). Despite quantitative discrepancies—notably at 19ºC where the model predicted a polymorphic population, but the data indicated otherwise (Fig 4e, f)—it correctly predicted observed changes in genetic frequencies across most temperatures, thus suggesting that temperature-dependent selection acting on G × E r-TPC variation can drive adaptive evolution in population genetic makeup.

Interestingly, the results of this experiment were also consistent with our estimated predicted responses to selection (cf Fig 3 and Fig 4): lower temperatures led to higher frequencies for the CU4106 genotype, which shows lower E_a and CT_{min}, compared to AXS (Fig 4d), while at higher temperatures, there was selection in favor of AXS, so that the ensuing population should have an average r-TPC with higher E_a (Fig 4d) as well. Therefore, such temperature-dependent selection on r-TPC G × E variation could lead to rapid r-TPC evolution through clonal sorting which could be predictable in nature (but see Nosil et al., 2018 for a counterpoint). Naturally, our lab-based study by necessity simplifies the complexities of how organisms contend with nature. Nonetheless, our experimental test of our mathematical predictions provides an important proof of principle in predicting evolutionary responses to a warming climate.

DISCUSSION

Our study reveals genetic variation in r-TPCs (Fig 2). While >70% of all TPC variation is

environmental (E), TPCs remain highly heritable (H^2>0.7, with G+G × E~18%) once controlled for inter-treatment and replicate variability, thus allowing selection to shape r-TPCs in new climates. We also show that different r-TPC shape parameters (Fig 1b) are under different selection regimes (Fig 3), and this selection is temperature-dependent, in some cases flipping from negative to positive with temperature (Fig 3). These temperature-dependent selection regimes should result in lower CT_{min}, r_{peak}, and E_a at cold temperatures while warmer temperatures should favor higher r_{peak} and E_a with no discernible effect on T_{opt} (Fig 3). Lastly, we show that G × E interactions are prevalent in these r-TPCs (Fig 1), which in turn can lead to rapid—but predictable—shifts in population genetic makeup across temperatures (Fig 4), and suggests that plasticity will help drive thermal adaptation (Ghalambor et al., 2007).

While the evolution of microbial TPCs in deep evolutionary time is likely the product of adaptation to local habitats (Kontopoulos et al., 2020; Phillips et al., 2014), how r-TPCs will adapt to rising temperatures is an open question. The 'Colder-is-Better' (CIB) hypothesis posits that rising temperatures reduce growth, leading to the evolution of lower r_{peak} in a warming world (J. Kingsolver & Huey, 2008). Conversely, the Warmer-Is-Better (WIB) hypothesis posits that growth increases in warmer temperatures, leading to TPCs with higher r_{peak} (Frazier et al., 2006; Pawar et al., 2015). Lastly, the Generalist-Specialist-Tradeoff (GST) hypothesis posits that species either exhibit rapid growth within a narrow temperature range (i.e., temperature specialists), or slower growth over a broader temperature range (i.e., temperature generalists) so that higher r_{peak} should also result in higher CT_{min} and lower CT_{max} (Seebacher et al., 2015). There is evidence supporting all three hypotheses (DeLong et al., 2018; Kontopoulos et al., 2020), but most of it comes from inter-species comparisons that overlook intra-specific variation and genetic associations between shape parameters, and therefore cannot readily make

247 predictions about r-TPC evolutionary trajectories for any given species. Without accounting for
248 genetic associations, our results would suggest, based on selection alone, support for WIB, with
249 clear directional selection for higher r_{peak} and E_a under warming climates (Fig 3a, b).
250 Accounting for genetic associations, however, showed support for multiple hypotheses
251 simultaneously, suggesting a more complex and nuanced evolutionary r-TPC response than
252 currently predicted by theory. Indeed, our analyses supported WIB, as warming should favor r-
253 TPCs with high r_{peak} and high E_a (Fig 3f, g), while countering GST, as there was no selection in
254 favor of higher CT_{min} with higher r_{peak} (Fig 3f, g). Lastly, T_{opt} was predicted to respond the least
255 to temperature (Fig 3g), as it showed only a small predicted decrease in colder temperatures
256 (likely though indirect selection)—which is arguably in support of CIB—except >30ºC, in
257 which case T_{opt} showed no clear pattern of evolutionary response to temperature —arguably
258 against WIB. Thus, like many studies, our ability to make predictions is context specific, and
259 identifying those contexts (e.g., temperature) remains an important avenue for future work. Our
260 results clearly emphasize the importance of intraspecific variation and genetic associations to
261 predict r-TPC evolution, and both support and generalize existing TPC evolution hypotheses.
262 We also uncovered an interesting mechanism of rapid thermal adaptation whenever there
263 is G × E in r-TPCs. While adaptation requires sufficient genetic variation upon which to act, the
264 adaptive sorting of standing genetic variation often leads to a reduction in genetic variation,
265 which can slow down the adaptive process or even impede future adaptation altogether (Pauls et
266 al., 2013). Our results show that, in the presence of extensive G × E variation in r-TPCs, rapid
267 shifts in genetic makeup are possible (Fig 4), resulting in predictable and rapid local adaptation
268 to novel conditions—i.e., phenotypic plasticity can be adaptive in novel climates. However, in
269 our system, rising temperatures led to an initial increase in additive genetic variance t (as both

genotypes become prevalent, Fig 4e, f), which should facilitate adaptation, then a reduction in additive genetic variation (as genotype CU4106 becomes less prevalent, Fig 4e, f), which in turn could impede adaptive evolution in the future. It is unclear why at 19ºC AXS is absent from the experimental populations despite the model predicting that its presence, and otherwise good agreement between model and data at other temperatures. This temperature-dependent effect on population genetic makeup may have important but poorly understood consequences for the conservation of genetically depauperate species under warming whenever large amounts of G × E are expected (Pauls et al., 2013).

Using a phylogenetic approach, a recent study found that TPC adaptation in deep time likely occurred gradually across six different *Tetrahymena* species (Montagnes et al., 2022). While seemingly in contrast with our finding that r-TPCs can evolve rapidly through temperature-dependent selection on r-TPC G × E variation, we argue that the mechanism of r-TPC evolution uncovered here is likely only at play as a form of rapid evolutionary response to fast-changing environmental conditions, and may or may not result in longer term indefinite r-TPC change. Indeed, selection often "erases its traces" (Haller & Hendry, 2014) with selection most often being strongest in novel conditions and diminishing as populations adapt (Caruso et al., 2017). Montagnes *et al.* (2021) also found poor support for WIB (which they referred to as thermodynamic-constraint) in contrast with our findings, which show some level of support for WIB. However, their study did uncover mixed support for CIB (which they call biochemical-adaptation, or hotter is not better) and poor support for GST, as did we, suggesting that some of the evolutionary responses uncovered here may be constrained by evolutionary history in deep time.

Overall, TPCs control the fate of populations (Seebacher & Little, 2021; Sinclair et al., 2016), ecological interactions (Bideault et al., 2019; Enquist et al., 2015), food web structure and dynamics (Barbour & Gibert, 2021; Gibert et al., 2022), and ecosystem processes (Antiqueira et al., 2018; Gibert et al., 2015). Yet, TPC evolution in a rapidly warming world remains a conspicuous unknown. Here, we shed light on how r-TPC intraspecific variation drives temperature-dependent evolution in a microbial r-TPC, as well as its consequence for rapid shifts in population genetic makeup that either facilitates or precludes future thermal adaptation. In doing so, we emphasize the importance of temperature in mediating rapid microbial evolutionary change as we grapple with understanding and predicting how organisms in the planet may respond to an increasingly warm world.

METHODS

Tetrahymena thermophila genotypes

We quantified intraspecific variation in r-TPCs in the protist *Tetrahymena thermophila*—a freshwater species that is distributed across the eastern United States (Zufall et al., 2013) and part of a genus of cosmopolitan distribution and importance (Lynn & Doerder, 2012). We used 22 unique *T. thermophila* genotypes: 19 from the Cornell Tetrahymena Stock Center and 3 strains from the Chalker lab (Washington University, Appendix S5). The genotypes vary in geographic origin and have specific genetic differences (Appendix S5). Our goal in using these genotypes was simply to have a source of genetic variation, not to select any particular genotypes on the basis of their functional significance. Because most of these genotypes are derived from laboratory cultures, this assemblage of genotypes likely harbors—collectively—less genetic variation than would be found in natural isolates from across the species' distribution (Zufall et

al., 2013). Upon reception, we transferred the cultures from axenic Proteose Peptone growth medium to Timothy Hay growth medium inoculated with a bacterial community from Duke Forest Gate 9 pond/Wilbur pond (Lat 36.013914, Long -78.979720, fully described elsewhere (Rocca et al., 2022) and a wheat kernel as a Carbon source (Altermatt et al., 2015). We maintained these stock cultures in Percival (Perry, IA) AL-22 growth chambers under light (12hr day-night cycle) and temperature controlled conditions (22°C) in 250mL borosilicate jars filled with 150mL of liquid medium. Because *T. thermophila* is a natural bacterivore, these experimental conditions are more realistic than purely axenic ones.

Quantifying TPCs and TPC shape parameters

We quantified the r-TPCs of all genotypes in 3cm diameter Petri dish microcosms with 3mL of growth medium through growth assays at seven temperatures (13, 19, 22, 25, 30, 32, 38°C), each replicated six times, totaling 1056 microcosms. We chose these temperatures because they capture the range of temperatures at which *T. thermophila* is known to grow well (Zufall et al., 2013). Microcosms were initialized by pipetting three individual cells from stock cultures under a scope (Leica stereomicroscope model M205C) and allowing them to grow for 24hrs, after which we censused the microcosms through whole-population counts under the scope, and calculated intrinsic growth rate, *r*, as log(final density/initial density)/time (Voronov, 2005; Wieczynski et al., 2021), with time = 1 day. We fitted a Sharpe-Schoolfield model ("nls.multstart" v1.3.0 package in R, (Padfield, 2023)) to obtain r-TPC shape parameters CT_{min} (minimum temperature at which the population can grow), CT_{max} (maximum temperature at which the population can grow), r_{peak} (maximum *growth rate*), T_{opt} (temperature at which r_{peak} is achieved), E_a (thermal sensitivity of the rising portion of the TPC) and E_d (thermal sensitivity of

the declining portion of the r-TPC, Fig 1b). Only parameters E_a, r_{peak}, CT_{min} and T_{opt} could be unequivocally estimated with our data, as fits were less well constrained at higher temperatures, and so we focused all subsequent analyses on those (Fig 1b). These parameters also control the rising portion of the r-TPC in the so-called 'operational temperature range' (DeLong et al., 2017; Smith et al., 2021), which also is the temperature range within which ecological responses to temperature are expected for organisms in their native geographic ranges.

Quantifying sources of phenotypic variation in r-TPCs and r-TPC heritability

To address whether and how r-TPCs may adapt to changing temperatures, we quantified standing genetic variation in r-TPC shape and how much of this variation was heritable. To do so, we estimated how much of the total observed r-TPC variation was explained by environmental variation (E), genetic variation (G) or Gene-by-Environment interactions (G × E, Fig 1c-e). The shape of r-TPCs are often assumed to be controlled by plastic physiological responses as a single genotype can often express an entire r-TPC ((J. G. Kingsolver et al., 2004), Fig 1c). We therefore expected to find a large amount of E. However, different genotypes may still express different TPCs (Singleton et al 2021, Fig 1d), and those could do so differentially across temperatures, leading to both G and G × E ((Ørsted et al., 2019), Fig 1e).

We estimated E, G and G × E using the function *gxeVarComps*() in R package statgenGxE v1.0.5. To do so, the procedure fits two models: first, it fits a fixed effects linear model with *r* as the response variable, and temperature, genotype, and the interaction between temperature and genotype as predictors to calculate effect sizes, significance levels, and Best Linear Unbiased Estimators (BLUEs, (Baksalary & Puntanen, 1990; Henderson, 1975)). BLUEs are subsequently used to calculate r-TPC broad-sense heritability (see below). Second, it re-fits the model with all terms as random effects to calculate the variance component of each term (i.e.,

G, E and G × E) and Best Linear Unbiased Predictors (BLUPs, (Henderson, 1975)), which are also subsequently used in the calculation of heritability. Using function *H2cal*() in R package inti v0.6.2 we calculated the broad-sense heritability (H^2) in three ways: 1) standard heritability, whereH^2=G/P, P = G+(G×E/m)+(ResidVar/(m*r)), *m* is the number of temperature treatments and *r* the number of replicates (which accounts for inter-treatment and replicate variability , in ways that G/P does not, (Baksalary & Puntanen, 1990; Henderson, 1975)), 2) *Cullis* heritability, where H^2= 1-vBLUE/2G, and vBLUE is the mean variance of the difference of two BLUEs (Cullis et al., 2006), and, 3) *Piepho* heritability, where H^2= G/(G+vBLUP), and vBLUP is the mean variance of a difference of two BLUPs (Piepho & Möhring, 2007).

Consequences of G: selection on r-TPC shape parameters and evolutionary potential

To understand how TPCs might evolve in different temperatures, we assessed: 1) selection direction/form and magnitude on TPC shape parameters, 2) the impact of temperature on such selection, and, 3) potential evolution of shape parameters under these selection regimes. We measured selection in two different ways: one that neglects genetic correlations between shape parameters but can be used to estimate non-linear selective effects (e.g., stabilizing selection), and one that accounts for genetic correlations but neglects non-linear terms but enables predictions of evolutionary potential. The first approach answered the first two questions while the second approach complemented the answer to the second question and addressed the third. In doing so, we are explicitly quantifying how selection on r-TPC shape parameters changes across temperatures, or what MacColl (2011) called “eco-evo landscapes” (MacColl, 2011).

In the first approach, we quantified the relationship between parameter values and absolute fitness—estimated here as, *r*—which is often assumed to be a suitable proxy for absolute fitness (Lande, 1976, 1979). This is because *r* reflects the birth and death rates per individual, two important fitness components (Lande, 1982; Partridge & Harvey, 1988). We considered three temperature ranges: low (<20°C), medium (between 20°C and 30°C), and high (>30°C). For each temperature range, we considered the relationship between *r* and the observed parameter value across genotypes (i.e., the adaptive landscape) (Lande, 1976, 1979). A positive relationship would be evidence of positive directional selection, a negative relationship, evidence of negative directional selection, and the absence of a relationship would occur whenever there is no directional selection. Stabilizing selection would result in a hump-shaped concave-down relationship, with intermediary values having higher fitness than extreme values, and disruptive selection with a concave-up relationship where extreme values have higher fitness (Lande & Arnold, 1983). We analyzed these data using polynomial regression in R v4.3.1 with *r* as the response variable, both linear and quadratic terms for the shape parameter and temperature as explanatory variables with additive effects, an interaction between the linear and quadratic effects of the shape parameter with temperature (See Appendices S1-S4). We doubled our quadratic regression coefficients (Stinchcombe et al., 2008).

To predict possible r-TPC shape evolution across temperatures and evaluate the effects of the genetic association among shape parameters in this evolutionary response, we used the modified **G**-matrix approach proposed by Stinchcombe *et al.* (2014). This approach fuses the multivariate breeder's (Lande, 1979) and Price's (Price, 1972) equations to estimate the direct (i.e., acting on the focal trait) and indirect effects of selection (i.e., acting on another trait the focal trait is genetically linked to) on an evolving population. The potential evolutionary

response of each r-TPC shape parameter to natural selection, $\mathbf{\Delta z}$, is derived from the covariance of the parameters with a measure of fitness. In practical terms, we estimated the additive genetic variance-covariance matrix, **G**, of all shape parameters, and the mean-standardized *r* as a measure of fitness, as done before (Lande 1976, 1972, 1989). We then created a $\mathbf{G_w}$-matrix, which includes **G** and a vector of predicted trait change, $\mathbf{\Delta z}$, as the last column and row. $\mathbf{\Delta z}$ is defined element-wise as $\Delta z_i = cov_a(w_i, z_i)$, with cov_a being the additive genetic covariance, w_i the relative fitness of the i-th shape parameter, and z_i the *i*-th shape parameter. Because the Δz_i calculated in this way is equivalent to the genetic selection differentials, we can then calculate the selection gradient as $\mathbf{\beta} = \mathbf{G_w}^{-1} \mathbf{\Delta z}$. The sign of Δz_i indicates the direction of the response. Alignment between Δz_i and β_i indicates direct responses to selection (Hansen and Houle 2008), that is, shape parameters that directly respond to selection as imposed by temperature, while misalignment would be indicative of indirect selection through correlated responses with other shape parameters. This approach correctly estimates $\mathbf{\Delta z}$ even in the absence of information on all pleiotropic effects in the system, while also estimating selection on each trait individually (Heath & Stinchcombe, 2014; Stinchcombe et al., 2014). Furthermore, $\mathbf{\beta}$ estimated in this way controls for the potential effects of environmentally induced trait-fitness covariances.

To calculate **G**, for each temperature, we compiled all r-TPC shape parameters and *r* for each genetic variant and calculated the between-genotype covariance matrix, **L.** For lines derived from the same population, **L** is proportional to the additive genetic covariance matrix of the original population, or $\mathbf{G_r}$. As inbreeding tends to increase between-genotype genetic variation due to drift, **L** is inflated in relation to **G** by a factor equal to two times the inbreeding coefficient, *F* (Falconer & Mackay, 1996). Genetic correlation among traits were obtained by estimating the correlation version of **G** as $\mathbf{G_{cor}} = \mathbf{SGS}$ where **S** is a diagonal matrix containing the

inverse of each trait's standard deviation. We estimated uncertainty using a Bayesian posterior sample of covariance matrices as implemented in the evolqg v3.0 package (Melo et al. 2015). This method derives the covariance matrices analytically from a multivariate normal likelihood function and an inverse Wishart prior (Murphy 2012). We then took 1000 posterior samples for $\mathbf{G_w}$ and derived statistics for $\mathbf{\Delta z}$, $\boldsymbol{\beta}$ and $\mathbf{G}$. To evaluate if $\mathbf{\Delta z}$, $\boldsymbol{\beta}$ and $\mathbf{G_{cor}}$ estimates were statistically meaningful, we inspected the 95% maximum density interval to evaluate if the posterior distribution significantly overlapped with the expected value due to lack of signal (value=0).

Experimental test of consequences of G × E for population genetic makeup across temperatures

If r-TPCs show G × E in shape, slight differences in intrinsic growth rates can lead to temperature-mediated clonal sorting (Fig 4a, b). We assessed how differences in r-TPCs across genotypes could influence thermal adaptation through sorting of standing variance using the coefficient of selection, *s*, which equals 1- w, where w is the relative fitness of each genotype (measured as the quotient of the *r* of each focal genotype, Fig 4d). The coefficient of selection measures the magnitude of selection acting against a given genotype relative to the focal genotype; the larger the value of *s*, the stronger the selection against the given genotype. Differences in *s* across genotypes and temperatures would indicate large potential for temperature-mediated clonal sorting.

We then tested whether temperature-mediated clonal sorting occurs by setting up an experimental evolution assay that competed two fluorescently marked strains that showed significantly different in r-TPCs and relative fitness (AXS and CU4106, Fig 4d, Fig4d inset) across six temperature treatments (19, 22, 25, 30, 32, 38ºC) each replicated seven times, with

additional single-strain controls per temperature. Microcosms were initialized at equal densities (5 individuals per genotype) in 3cm diameter Petri dishes. We added $CdCl_2$ on days 2 and 7 to induce fluorescence and counted on days 3 and 8. Fluorescently tagged genotypes may lose their ability to fluoresce over time—however, they carry a Paromomycin resistance gene so that fluorescing individuals can be selected for through Paromomycin exposure. We treated the microcosms with 100µg/mL of Paromomycin prior to censusing, then used a Novocyte 2000R flow cytometer (Agilent, Santa Clara, CA) to count individual cells and estimate relative frequencies based on fluorescence (See Appendix S6 and Appendix S7). Because antibiotics can influence the protists and the bacterial communities they feed on in multiple ways, we replicated the entire experiment in Paromomycin-free conditions, but this did not qualitatively alter our results (see Appendix Fig S8).

To confirm fluorescence of the two strains (Fig 4c), cells were mounted on glass slides with mounting medium (Winey et al., 2012). Images were taken with a Leica Thunder Cell Culture inverted microscope equipped with an HC PL APO 63X/1.40 N.A. oil-immersion objective lens. Fluorescent signals were captured using a 510-nm excitation laser and a 535/15-nm emission filter for YFP (expressed in genotype AXS), and a 395-nm excitation laser and a Leica DFT51011 quad-band filter set for autofluorescence (exhibited by both genotypes). All images were captured at a single Z plane using the same exposure settings; the resulting images were processed in ImageJ (see Fig 4c and Appendix Figure S9).

Last, observed changes in genetic frequencies were compared to predicted frequencies by a modified version of a classic model of genetic evolution in discrete time parameterized with the r-TPC of each strain in the experimental evolution assay (Fig 4f). The model tracks the frequency of each strain f_i, and assumes that their absolute fitness, W_i, is a function of their

476 reproductive output (r), following early work by Lande (Lande, 1976, 1979). The frequency of
477 each strain in the population is then determined by the classic recursive equation, $f_i(t+1) =$
478 $f_i(t)W_i/\bar{W}$ [Eq 1.], where $\bar{W}$ is the average fitness in the population ($\sum_{i=1}^{n} f_i r_i$), such that $W_i/\bar{W}$ is
479 the relative fitness of the i-th strain. Alternatively, we can calculate the fitness of each strain
480 relative to that of a focal strain (we call it S_{focal}, Fig 4d inset). Then the relative fitness equation
481 becomes $W_i/\bar{W}_{S_{focal}}$. In our experiment, we only have two strains (AXS and CU4106), so either
482 strain can be the focal strain, but this choice does not alter the evolutionary dynamics. Our focal
483 strain was CU4016. We used each strain's r-TPC (Fig 4d) to calculate the relative fitness of each
484 strain as $W_{\mathrm{AXS}}/W_{\mathrm{CU4016}}$ for AXS and $W_{\mathrm{CU4016}}/W_{\mathrm{CU4016}}$ for CU4106 (Fig 4d, inset) –thus
485 replacing each strain's fitness, W_i, with their r-TPC (Lande 1976). We then replaced these
486 empirically parameterized measures of relative fitness in our recursive equation (Eq 1.) and
487 numerically solved the recursive equation over time to make testable predictions of how genetic
488 frequencies should change across temperatures. Despite this model not accounting for density,
489 frequency, and other forms of selection and ecological processes, is does a good job at
490 qualitatively reproducing the observed evolutionary dynamics (Fig 4e, f), therefore supporting
491 the hypothesis that observed shifts in genetic frequencies are due to GxE in r-TPCs and
492 temperature-mediated selection.
493
494
495
496

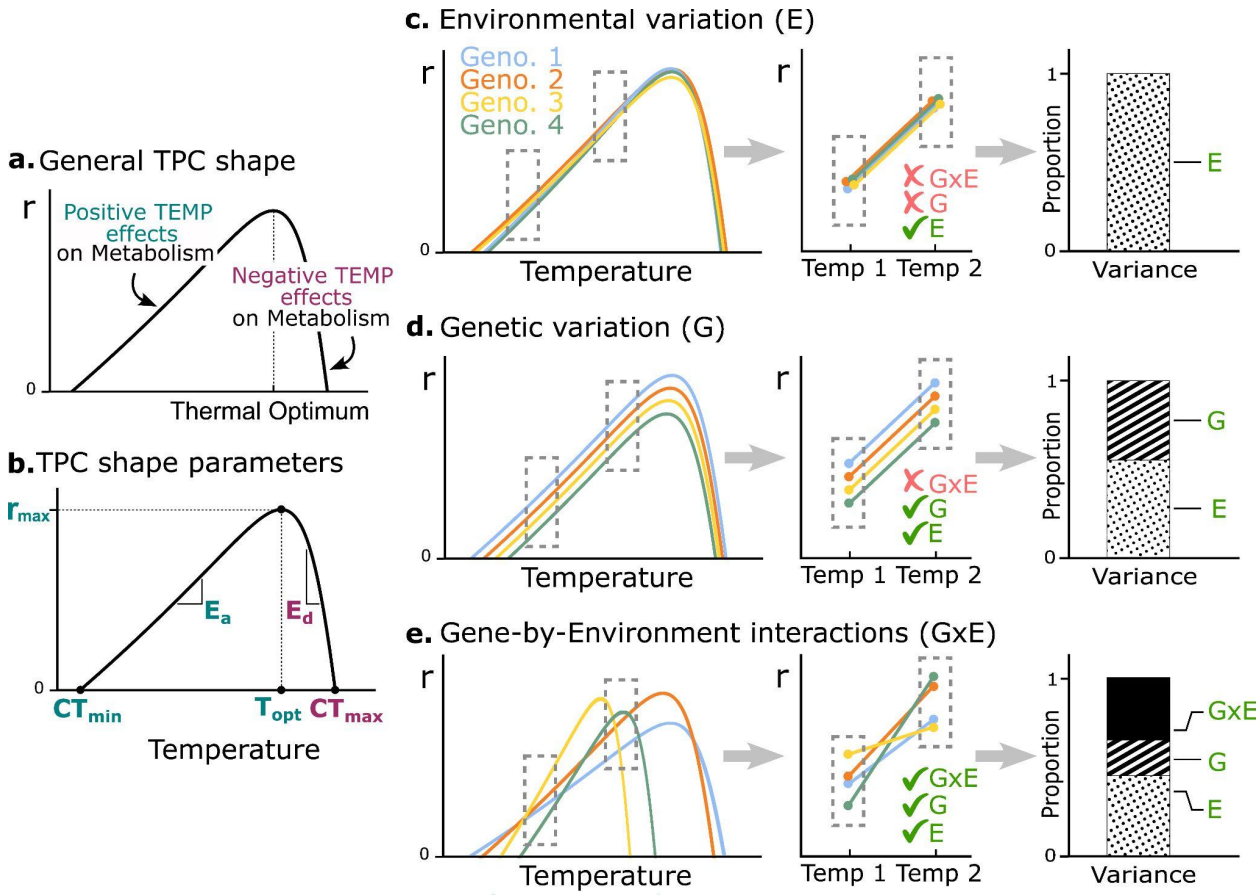

Fig. 1: **a.** General shape of the r-TPC. **b.** r-TPC shape parameters. Blue-colored shape parameters indicate those measured in this study, namely, r_{peak}, E_a, CT_{min} and T_{opt}. **c.** Environmental variation (E) in r-TPCs results from the expression of a different *r* across temperatures. In the classic reaction norm approach, this would be observed as different *r* values across temperatures, but equal across genotypes within temperatures (middle panel). **d.** Genetic variation (G) in r-TPCs occurs whenever different genotypes express TPCs with different heights, such that in the classic reaction norm approach observed *r* values vary across but in such a way that the slope of the effect of the genotype on *r* is additive (middle panel). **e.** Gene-by-Environment interactions (G × E) occur whenever TPCs vary in both heights and slopes across genotypes, such that, in the classic reaction norm approach, *r* varies across genotypes and temperatures in a multiplicative fashion.

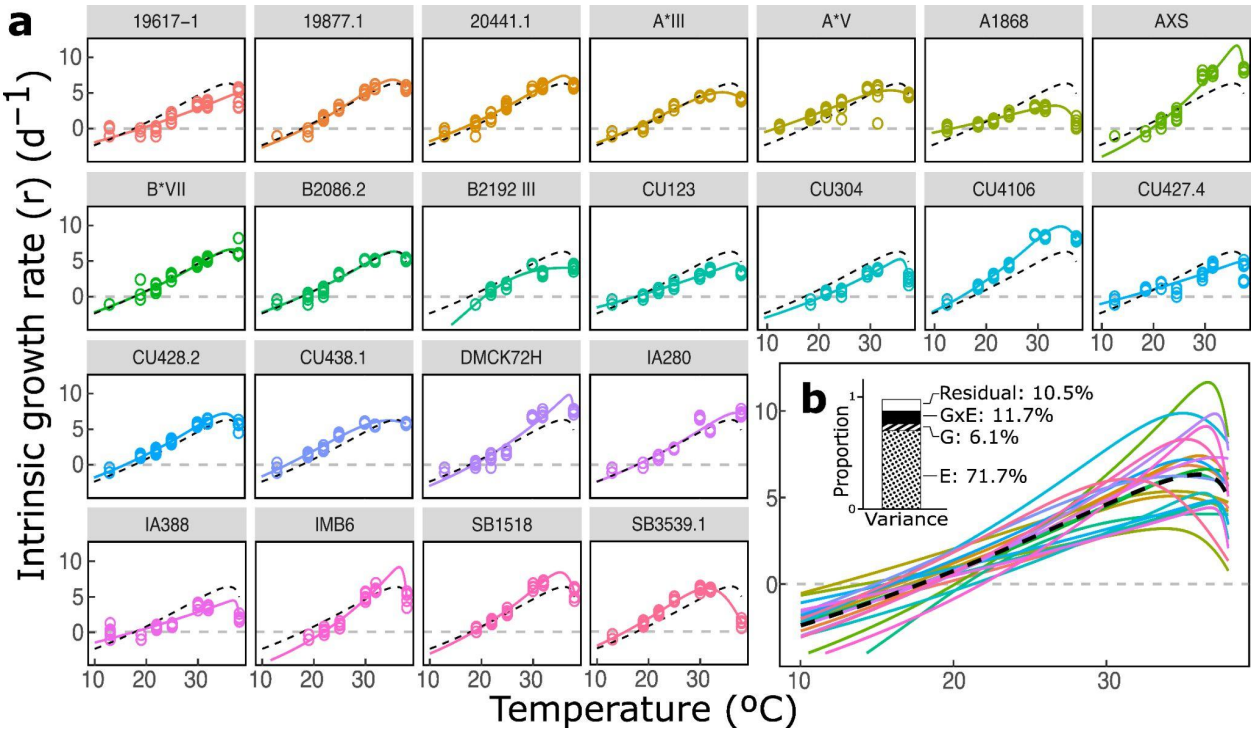

Fig. 2: a. Observed r-TPCs for all 22 genotypes. Dots represent observed *r* values, bold lines represent Sharpe-Schoolfield model fits, and dash lines represent average TPCs across all experimental genotypes. **b.** All 22 TPCs are superimposed and dashed lines represent the average r-TPC. Inset: amount of variation due to residual, G × E, G, and E effects.

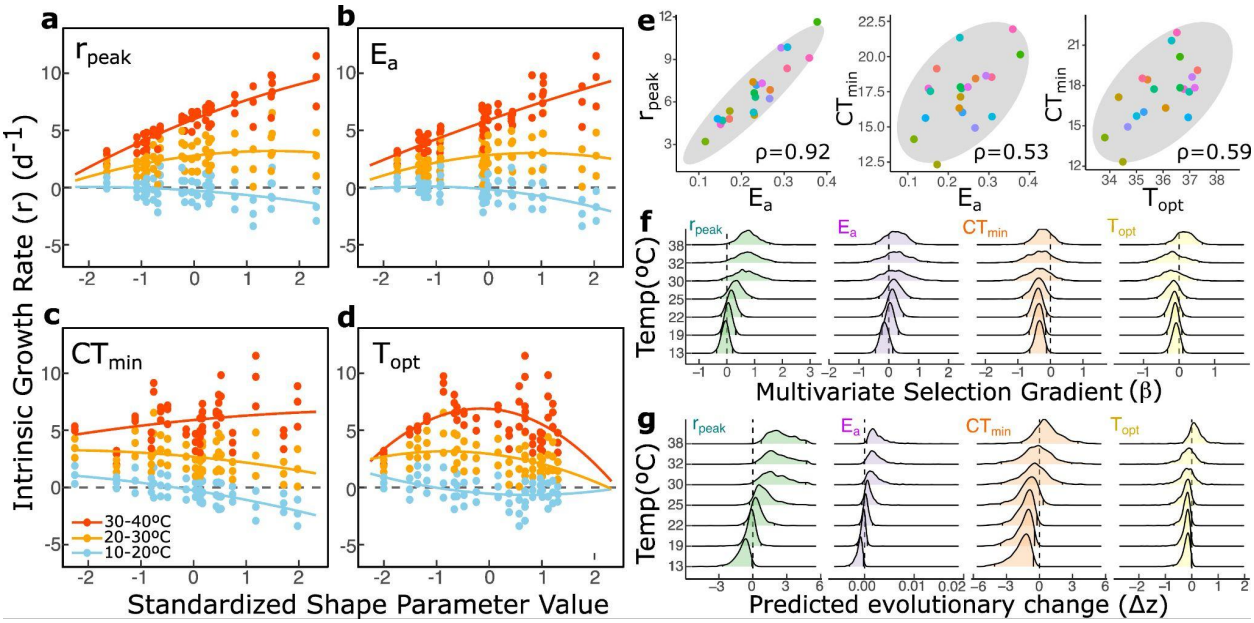

Fig. 3: a. Estimated adaptive landscape across temperatures (i.e., change in fitness with a change in the underlying shape parameter) for r_{peak}. Color indicates temperature (blue: 10–20ºC, yellow: 20–30ºC, red: 30–40ºC) **b.** As in **a**, but for E_a. **c.** As in **a**, but for CT_{min}. **d.** As in **a**, but for T_{opt}. **e.** Observed genetic associations between shape parameters. Each dot is a genotype color-coded as in Fig. 2. In gray, 95% confidence ellipses. ρ represents correlation coefficients. **f.** Estimated multivariate selection coefficient (**β,** 95% maximum density intervals) for all shape parameters across temperatures, or eco-evo landscapes (MacColl, 2011). **g.** Predicted evolutionary change (**Δz,** 95% maximum density intervals) for all shape parameters, across temperatures.

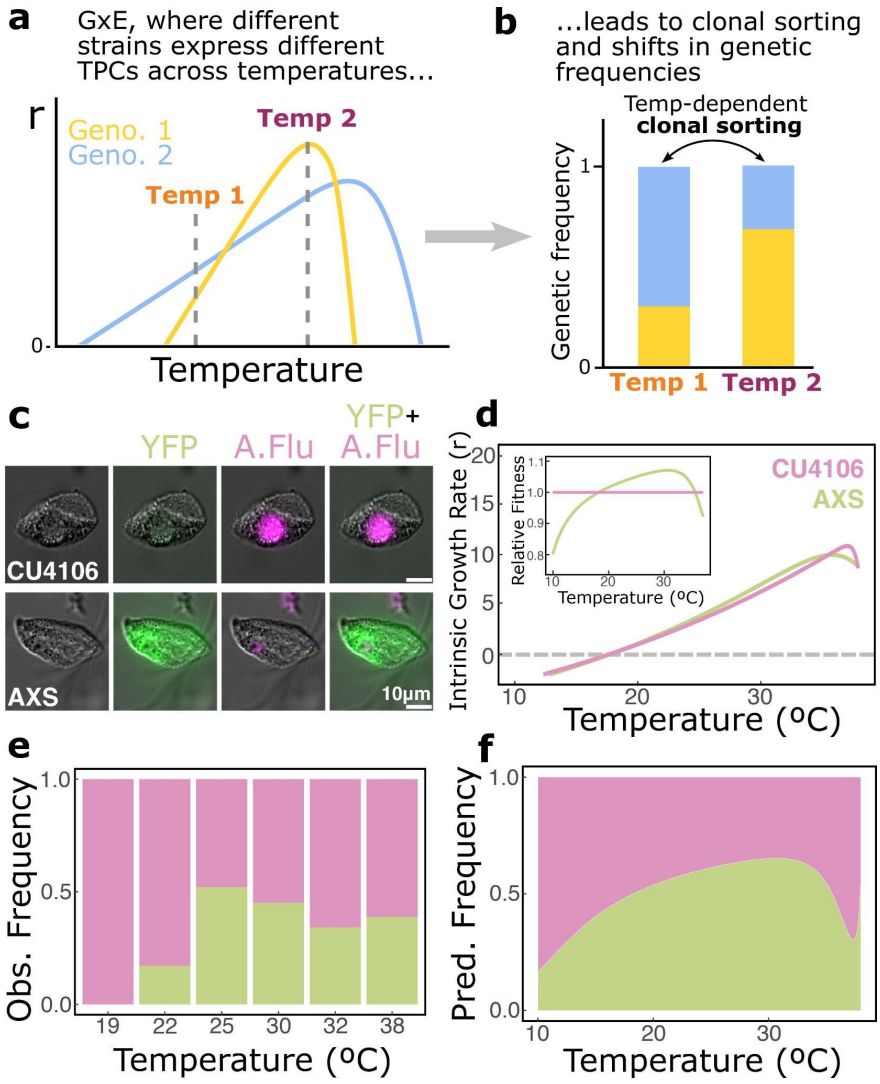

Fig. 4: a. G × E variation in r-TPCs leads to differential growth of each genotype across temperatures. **b.** Differential growth across temperatures leads to clonal sorting and rapid shifts in genetic frequencies across temperatures. **c.** First column: Differential Interference Contrast (DIC) microscopy for two genotypes of the protist *Tetrahymena thermophila* (CU4106 and AXS). Second column: fluorescence microscopy image overlayed on DIC. Only AXS fluoresces (green) due to the expression of Yellow Fluorescent Protein (YFP). Third column: as in the second column, but for autofluorescence (A. Flu, in pink), which both genotypes exhibit. Fourth column: Overlayed DIC, YFP and A.Flu images showing how the different strains fluoresce once all sources of fluorescence are accounted for. **d.** r-TPC for genotypes CU4106 and AXS. Inset: Measures of relative fitness for both CU4106 and AXS. This predicts an increase in AXS frequency relative to CU4106 at intermediate temperatures relative to low or high temperatures. **e.** Observed genetic frequencies across temperatures. **f.** Predicted genetic frequencies across temperatures.

REFERENCES

Altermatt, F., Fronhofer, E. A., Garnier, A., Giometto, A., Hammes, F., Klecka, J., Legrand, D., Mächler, E., Massie, T. M., Pennekamp, F., Plebani, M., Pontarp, M., Schtickzelle, N., Thuillier, V., & Petchey, O. L. (2015). Big answers from small worlds: A user's guide for protist microcosms as a model system in ecology and evolution. *Methods in Ecology and Evolution*, *6*(2), 218–231. https://doi.org/10.1111/2041-210X.12312

Amarasekare, P., & Savage, V. (2012). A Framework for Elucidating the Temperature Dependence of Fitness. *The American Naturalist*, *179*(2), 178–191. https://doi.org/10.1086/663677

Angilletta, M. J. (2009). *Thermal Adaptation: A Theoretical and Empirical Synthesis*. OUP Oxford.

Antiqueira, P. A. P., Petchey, O. L., & Romero, G. Q. (2018). Warming and top predator loss drive ecosystem multifunctionality. *Ecology Letters*, *21*(1), 72–82. https://doi.org/10.1111/ele.12873

Arrigo, K. R. (2005). Marine microorganisms and global nutrient cycles. *Nature*, *437*(7057), Article 7057. https://doi.org/10.1038/nature04159

Baksalary, J. K., & Puntanen, S. (1990). Characterizations of the best linear unbiased estimator in the general Gauss-Markov model with the use of matrix partial orderings. *Linear Algebra and Its Applications*, *127*, 363–370. https://doi.org/10.1016/0024-3795(90)90349-H

Barbour, M. A., & Gibert, J. P. (2021). Genetic and plastic rewiring of food webs under climate change. *Journal of Animal Ecology*, *90*(8), 1814–1830. https://doi.org/10.1111/1365-2656.13541

Bar-On, Y. M., & Milo, R. (2019). The Biomass Composition of the Oceans: A Blueprint of Our Blue Planet. *Cell*, *179*(7), 1451–1454. https://doi.org/10.1016/j.cell.2019.11.018

Bar-On, Y. M., Phillips, R., & Milo, R. (2018). The biomass distribution on Earth. *Proceedings of the National Academy of Sciences*, *115*(25), 6506–6511. https://doi.org/10.1073/pnas.1711842115

Barrett, R. D. H., & Schluter, D. (2008). Adaptation from standing genetic variation. *Trends in Ecology & Evolution*, *23*(1), 38–44. https://doi.org/10.1016/j.tree.2007.09.008

Barton, S., Jenkins, J., Buckling, A., Schaum, C.-E., Smirnoff, N., Raven, J. A., & Yvon-Durocher, G. (2020). Evolutionary temperature compensation of carbon fixation in marine phytoplankton.

Ecology Letters, *23*(4), 722–733. https://doi.org/10.1111/ele.13469

Bideault, A., Loreau, M., & Gravel, D. (2019). Temperature Modifies Consumer-Resource Interaction Strength Through Its Effects on Biological Rates and Body Mass. *Frontiers in Ecology and Evolution*, *7*. https://www.frontiersin.org/articles/10.3389/fevo.2019.00045

Bond-Lamberty, B. (2018). New Techniques and Data for Understanding the Global Soil Respiration Flux. *Earth's Future*, *6*(9), 1176–1180. https://doi.org/10.1029/2018EF000866

Brown, J. H., Gillooly, J. F., Allen, A. P., Savage, V. M., & West, G. B. (2004). Toward a Metabolic Theory of Ecology. *Ecology*, *85*(7), 1771–1789. https://doi.org/10.1890/03-9000

Caruso, C. M., Martin, R. A., Sletvold, N., Morrissey, M. B., Wade, M. J., Augustine, K. E., Carlson, S. M., MacColl, A. D. C., Siepielski, A. M., & Kingsolver, J. G. (2017). What Are the Environmental Determinants of Phenotypic Selection? A Meta-analysis of Experimental Studies. *The American Naturalist*, *190*(3), 363–376. https://doi.org/10.1086/692760

Cullis, B. R., Smith, A. B., & Coombes, N. E. (2006). On the design of early generation variety trials with correlated data. *Journal of Agricultural, Biological, and Environmental Statistics*, *11*(4), 381–393. https://doi.org/10.1198/108571106X154443

Davidson, E. A., & Janssens, I. A. (2006). Temperature sensitivity of soil carbon decomposition and feedbacks to climate change. *Nature*, *440*(7081), Article 7081. https://doi.org/10.1038/nature04514

DeLong, J. P., Bachman, G., Gibert, J. P., Luhring, T. M., Montooth, K. L., Neyer, A., & Reed, B. (2018). Habitat, latitude and body mass influence the temperature dependence of metabolic rate. *Biology Letters*, *14*(8), 20180442. https://doi.org/10.1098/rsbl.2018.0442

DeLong, J. P., Gibert, J. P., Luhring, T. M., Bachman, G., Reed, B., Neyer, A., & Montooth, K. L. (2017). The combined effects of reactant kinetics and enzyme stability explain the temperature dependence of metabolic rates. *Ecology and Evolution*, *7*(11), 3940–3950. https://doi.org/10.1002/ece3.2955

Deutsch, C. A., Tewksbury, J. J., Huey, R. B., Sheldon, K. S., Ghalambor, C. K., Haak, D. C., & Martin,

P. R. (2008). Impacts of climate warming on terrestrial ectotherms across latitude. *Proceedings of the National Academy of Sciences*, *105*(18), 6668–6672. https://doi.org/10.1073/pnas.0709472105

Enquist, B. J., Norberg, J., Bonser, S. P., Violle, C., Webb, C. T., Henderson, A., Sloat, L. L., & Savage, V. M. (2015). Chapter Nine - Scaling from Traits to Ecosystems: Developing a General Trait Driver Theory via Integrating Trait-Based and Metabolic Scaling Theories. In S. Pawar, G. Woodward, & A. I. Dell (Eds.), *Advances in Ecological Research* (Vol. 52, pp. 249–318). Academic Press. https://doi.org/10.1016/bs.aecr.2015.02.001

Falkowski, P. G. (1994). The role of phytoplankton photosynthesis in global biogeochemical cycles. *Photosynthesis Research*, *39*(3), 235–258. https://doi.org/10.1007/BF00014586

Falkowski, P. G., Fenchel, T., & Delong, E. F. (2008). The Microbial Engines That Drive Earth's Biogeochemical Cycles. *Science*, *320*(5879), 1034–1039. https://doi.org/10.1126/science.1153213

Frankham, R. (2005). Stress and adaptation in conservation genetics. *Journal of Evolutionary Biology*, *18*(4), 750–755. https://doi.org/10.1111/j.1420-9101.2005.00885.x

Franks, S. J., Sim, S., & Weis, A. E. (2007). Rapid evolution of flowering time by an annual plant in response to a climate fluctuation. *Proceedings of the National Academy of Sciences*, *104*(4), 1278–1282. https://doi.org/10.1073/pnas.0608379104

Frazier, M. R., Huey, R. B., & Berrigan, D. (2006). Thermodynamics Constrains the Evolution of Insect Population Growth Rates: "Warmer Is Better." *The American Naturalist*, *168*(4), 512–520. https://doi.org/10.1086/506977

Geisen, S., Mitchell, E. A. D., Adl, S., Bonkowski, M., Dunthorn, M., Ekelund, F., Fernández, L. D., Jousset, A., Krashevska, V., Singer, D., Spiegel, F. W., Walochnik, J., & Lara, E. (2018). Soil protists: A fertile frontier in soil biology research. *FEMS Microbiology Reviews*, *42*(3), 293–323. https://doi.org/10.1093/femsre/fuy006

Ghalambor, C. K., McKAY, J. K., Carroll, S. P., & Reznick, D. N. (2007). Adaptive versus non-adaptive

phenotypic plasticity and the potential for contemporary adaptation in new environments. *Functional Ecology*, *21*(3), 394–407. https://doi.org/10.1111/j.1365-2435.2007.01283.x

Gibert, J. P., Dell, A. I., DeLong, J. P., & Pawar, S. (2015). Chapter One—Scaling-up Trait Variation from Individuals to Ecosystems. In S. Pawar, G. Woodward, & A. I. Dell (Eds.), *Advances in Ecological Research* (Vol. 52, pp. 1–17). Academic Press. https://doi.org/10.1016/bs.aecr.2015.03.001

Gibert, J. P., Grady, J. M., & Dell, A. I. (2022). Food web consequences of thermal asymmetries. *Functional Ecology*, *36*(8), 1887–1899. https://doi.org/10.1111/1365-2435.14091

Gillooly, J. F., Brown, J. H., West, G. B., Savage, V. M., & Charnov, E. L. (2001). Effects of size and temperature on metabolic rate. *Science (New York, N.Y.)*, *293*(5538), 2248–2251. https://doi.org/10.1126/science.1061967

Haller, B. C., & Hendry, A. P. (2014). Solving the paradox of stasis: Squashed stabilizing selection and the limits of detection. *Evolution; International Journal of Organic Evolution*, *68*(2), 483–500. https://doi.org/10.1111/evo.12275

Hansen, T. F., & Houle, D. (2008). Measuring and comparing evolvability and constraint in multivariate characters. *Journal of Evolutionary Biology*, *21*(5), 1201–1219. https://doi.org/10.1111/j.1420-9101.2008.01573.x

Heath, K. D., & Stinchcombe, J. R. (2014). Explaining Mutualism Variation: A New Evolutionary Paradox? *Evolution*, *68*(2), 309–317. https://doi.org/10.1111/evo.12292

Henderson, C. R. (1975). Best Linear Unbiased Estimation and Prediction under a Selection Model. *Biometrics*, *31*(2), 423–447. https://doi.org/10.2307/2529430

Hoffmann, A. A., & Sgrò, C. M. (2011). Climate change and evolutionary adaptation. *Nature*, *470*(7335), Article 7335. https://doi.org/10.1038/nature09670

Hu, S. K., Herrera, E. L., Smith, A. R., Pachiadaki, M. G., Edgcomb, V. P., Sylva, S. P., Chan, E. W., Seewald, J. S., German, C. R., & Huber, J. A. (2021). Protistan grazing impacts microbial communities and carbon cycling at deep-sea hydrothermal vents. *Proceedings of the National*

673 *Academy of Sciences*, *118*(29), e2102674118. https://doi.org/10.1073/pnas.2102674118
674 Intergovernmental Panel on Climate Change (IPCC). (2023). *Climate Change 2021 – The Physical*
675 *Science Basis: Working Group I Contribution to the Sixth Assessment Report of the*
676 *Intergovernmental Panel on Climate Change*. Cambridge University Press.
677 https://doi.org/10.1017/9781009157896
678 Jacob, S., & Legrand, D. (2021). Phenotypic plasticity can reverse the relative extent of intra- and
679 interspecific variability across a thermal gradient. *Proceedings of the Royal Society B: Biological*
680 *Sciences*, *288*(1953), 20210428. https://doi.org/10.1098/rspb.2021.0428
681 Kellermann, V., Chown, S. L., Schou, M. F., Aitkenhead, I., Janion-Scheepers, C., Clemson, A., Scott, M.
682 T., & Sgrò, C. M. (2019). Comparing thermal performance curves across traits: How consistent
683 are they? *Journal of Experimental Biology*, *222*(11), jeb193433.
684 https://doi.org/10.1242/jeb.193433
685 Kingsolver, J. G., Izem, R., & Ragland, G. J. (2004). Plasticity of Size and Growth in Fluctuating
686 Thermal Environments: Comparing Reaction Norms and Performance Curves. *Integrative and*
687 *Comparative Biology*, *44*(6), 450–460.
688 Kingsolver, J., & Huey, R. (2008). Size, temperature, and fitness: Three rules. *Evolutionary Ecology*
689 *Research*, *10*, 251–268.
690 Kirkpatrick, M., & Peischl, S. (2013). Evolutionary rescue by beneficial mutations in environments that
691 change in space and time. *Philosophical Transactions of the Royal Society B: Biological*
692 *Sciences*, *368*(1610), 20120082. https://doi.org/10.1098/rstb.2012.0082
693 Kling, J. D., Lee, M. D., Walworth, N. G., Webb, E. A., Coelho, J. T., Wilburn, P., Anderson, S. I., Zhou,
694 Q., Wang, C., Phan, M. D., Fu, F., Kremer, C. T., Litchman, E., Rynearson, T. A., & Hutchins, D.
695 A. (2023). Dual thermal ecotypes coexist within a nearly genetically identical population of the
696 unicellular marine cyanobacterium Synechococcus. *Proceedings of the National Academy of*
697 *Sciences*, *120*(47), e2315701120. https://doi.org/10.1073/pnas.2315701120
698 Kontopoulos, D.-G., Smith, T. P., Barraclough, T. G., & Pawar, S. (2020). Adaptive evolution shapes the

present-day distribution of the thermal sensitivity of population growth rate. *PLOS Biology*, *18*(10), e3000894. https://doi.org/10.1371/journal.pbio.3000894

Lande, R. (1976). Natural Selection and Random Genetic Drift in Phenotypic Evolution. *Evolution*, *30*(2), 314–334. https://doi.org/10.2307/2407703

Lande, R. (1979). Quantitative Genetic Analysis of Multivariate Evolution, Applied to Brain:body Size Allometry. *Evolution*, *33*(1Part2), 402–416. https://doi.org/10.1111/j.1558-5646.1979.tb04694.x

Lande, R. (1982). A Quantitative Genetic Theory of Life History Evolution. *Ecology*, *63*(3), 607–615. https://doi.org/10.2307/1936778

Lande, R., & Arnold, S. J. (1983). THE MEASUREMENT OF SELECTION ON CORRELATED CHARACTERS. *Evolution*, *37*(6), 1210–1226. https://doi.org/10.1111/j.1558-5646.1983.tb00236.x

Litchman, E., de Tezanos Pinto, P., Edwards, K. F., Klausmeier, C. A., Kremer, C. T., & Thomas, M. K. (2015). Global biogeochemical impacts of phytoplankton: A trait-based perspective. *Journal of Ecology*, *103*(6), 1384–1396.

Liu, L., Wang, Y., Zhang, D., Chen, Z., Chen, X., Su, Z., & He, X. (2020). The Origin of Additive Genetic Variance Driven by Positive Selection. *Molecular Biology and Evolution*, *37*(8), 2300–2308. https://doi.org/10.1093/molbev/msaa085

Lynn, D. H., & Doerder, F. P. (2012). The life and times of Tetrahymena. *Methods in Cell Biology*, *109*, 9–27. https://doi.org/10.1016/B978-0-12-385967-9.00002-5

MacColl, A. D. C. (2011). The ecological causes of evolution. *Trends in Ecology & Evolution*, *26*(10), 514–522. https://doi.org/10.1016/j.tree.2011.06.009

Malusare, S. P., Zilio, G., & Fronhofer, E. A. (2023). Evolution of thermal performance curves: A meta-analysis of selection experiments. *Journal of Evolutionary Biology*, *36*(1), 15–28. https://doi.org/10.1111/jeb.14087

Montagnes, D. J. S., Wang, Q., Lyu, Z., & Shao, C. (2022). Evaluating thermal performance of closely related taxa: Support for hotter is not better, but for unexpected reasons. *Ecological Monographs*,

92(3), e1517. https://doi.org/10.1002/ecm.1517

Nguyen, B.-A. T., Chen, Q.-L., He, J.-Z., & Hu, H.-W. (2020). Microbial regulation of natural antibiotic resistance: Understanding the protist-bacteria interactions for evolution of soil resistome. *The Science of the Total Environment*, *705*, 135882. https://doi.org/10.1016/j.scitotenv.2019.135882

NOAA. (n.d.). *NOAA NCEI U.S. Climate Normals Quick Access*. Retrieved January 23, 2024, from https://www.ncei.noaa.gov/access/us-climate-normals/#dataset=normals-monthly&timeframe=30&location=MA&station=USW00014739

Nosil, P., Villoutreix, R., de Carvalho, C. F., Farkas, T. E., Soria-Carrasco, V., Feder, J. L., Crespi, B. J., & Gompert, Z. (2018). Natural selection and the predictability of evolution in Timema stick insects. *Science (New York, N.Y.)*, *359*(6377), 765–770. https://doi.org/10.1126/science.aap9125

Ørsted, M., Hoffmann, A. A., Rohde, P. D., Sørensen, P., & Kristensen, T. N. (2019). Strong impact of thermal environment on the quantitative genetic basis of a key stress tolerance trait. *Heredity*, *122*(3), 315–325. https://doi.org/10.1038/s41437-018-0117-7

Padfield, D. (2023). *Robust Non-Linear Regression using AIC Scores* (1.3.0) [R].

Partridge, L., & Harvey, P. H. (1988). The Ecological Context of Life History Evolution. *Science*, *241*(4872), 1449–1455. https://doi.org/10.1126/science.241.4872.1449

Pauls, S. U., Nowak, C., Bálint, M., & Pfenninger, M. (2013). The impact of global climate change on genetic diversity within populations and species. *Molecular Ecology*, *22*(4), 925–946. https://doi.org/10.1111/mec.12152

Pawar, S., Dell, A. I., & Savage, V. M. (2015). Chapter 1—From Metabolic Constraints on Individuals to the Dynamics of Ecosystems. In A. Belgrano, G. Woodward, & U. Jacob (Eds.), *Aquatic Functional Biodiversity* (pp. 3–36). Academic Press. https://doi.org/10.1016/B978-0-12-417015-5.00001-3

Phillips, B. L., Llewelyn, J., Hatcher, A., Macdonald, S., & Moritz, C. (2014). Do evolutionary constraints on thermal performance manifest at different organizational scales? *Journal of Evolutionary Biology*, *27*(12), 2687–2694. https://doi.org/10.1111/jeb.12526

751 Piepho, H.-P., & Möhring, J. (2007). Computing Heritability and Selection Response From Unbalanced
752 Plant Breeding Trials. *Genetics*, *177*(3), 1881–1888. https://doi.org/10.1534/genetics.107.074229
753 Price, G. R. (1972). Extension of covariance selection mathematics. *Annals of Human Genetics*, *35*(4),
754 485–490. https://doi.org/10.1111/j.1469-1809.1957.tb01874.x
755 Rebolledo, A. P., Sgrò, C. M., & Monro, K. (2020). Thermal performance curves reveal shifts in optima,
756 limits and breadth in early life. *Journal of Experimental Biology*, *223*(22), jeb233254.
757 https://doi.org/10.1242/jeb.233254
758 Rocca, J. D., Yammine, A., Simonin, M., & Gibert, J. P. (2022). Protist Predation Influences the
759 Temperature Response of Bacterial Communities. *Frontiers in Microbiology*, *13*.
760 https://www.frontiersin.org/articles/10.3389/fmicb.2022.847964
761 Savage, V. M., Gillooly, J. F., Brown, J. H., West, G. B., & Charnov, E. L. (2004). Effects of Body Size
762 and Temperature on Population Growth. *The American Naturalist*, *163*(3), 429–441.
763 https://doi.org/10.1086/381872
764 Schoolfield, R. M., Sharpe, P. J. H., & Magnuson, C. E. (1981). Non-linear regression of biological
765 temperature-dependent rate models based on absolute reaction-rate theory. *Journal of Theoretical*
766 *Biology*, *88*(4), 719–731. https://doi.org/10.1016/0022-5193(81)90246-0
767 Schulte, P. M., Healy, T. M., & Fangue, N. A. (2011). Thermal Performance Curves, Phenotypic
768 Plasticity, and the Time Scales of Temperature Exposure. *Integrative and Comparative Biology*,
769 *51*(5), 691–702. https://doi.org/10.1093/icb/icr097
770 Seebacher, F., Ducret, V., Little, A. G., & Adriaenssens, B. (2015). Generalist–specialist trade-off during
771 thermal acclimation. *Royal Society Open Science*, *2*(1), 140251.
772 https://doi.org/10.1098/rsos.140251
773 Seebacher, F., & Little, A. G. (2021). Plasticity of Performance Curves in Ectotherms: Individual
774 Variation Modulates Population Responses to Environmental Change. *Frontiers in Physiology*,
775 *12*. https://www.frontiersin.org/articles/10.3389/fphys.2021.733305
776 Sinclair, B. J., Marshall, K. E., Sewell, M. A., Levesque, D. L., Willett, C. S., Slotsbo, S., Dong, Y.,

Harley, C. D. G., Marshall, D. J., Helmuth, B. S., & Huey, R. B. (2016). Can we predict ectotherm responses to climate change using thermal performance curves and body temperatures? *Ecology Letters*, *19*(11), 1372–1385. https://doi.org/10.1111/ele.12686

Singleton, A. L., Liu, M. H., Votzke, S., Yammine, A., & Gibert, J. P. (2021). Increasing temperature weakens the positive effect of genetic diversity on population growth. *Ecology and Evolution*, *11*(24), 17810–17816. https://doi.org/10.1002/ece3.8335

Smith, T. P., Clegg, T., Bell, T., & Pawar, S. (2021). Systematic variation in the temperature dependence of bacterial carbon use efficiency. *Ecology Letters*, *24*(10), 2123–2133. https://doi.org/10.1111/ele.13840

Stell, E., Warner, D., Jian, J., Bond-Lamberty, B., & Vargas, R. (2021). Spatial biases of information influence global estimates of soil respiration: How can we improve global predictions? *Global Change Biology*, *27*(16), 3923–3938. https://doi.org/10.1111/gcb.15666

Stinchcombe, J. R., Agrawal, A. F., Hohenlohe, P. A., Arnold, S. J., & Blows, M. W. (2008). Estimating Nonlinear Selection Gradients Using Quadratic Regression Coefficients: Double or Nothing? *Evolution*, *62*(9), 2435–2440. https://doi.org/10.1111/j.1558-5646.2008.00449.x

Stinchcombe, J. R., Simonsen, A. K., & Blows, Mark. W. (2014). ESTIMATING UNCERTAINTY IN MULTIVARIATE RESPONSES TO SELECTION. *Evolution*, *68*(4), 1188–1196. https://doi.org/10.1111/evo.12321

Trumbore, S. (2006). Carbon respired by terrestrial ecosystems – recent progress and challenges. *Global Change Biology*, *12*(2), 141–153. https://doi.org/10.1111/j.1365-2486.2006.01067.x

Voronov, D. A. (2005). [Calculating the intrinsic growth rate: Comparison of definition and model]. *Zhurnal Obshchei Biologii*, *66*(5), 425–430.

Wieczynski, D. J., Singla, P., Doan, A., Singleton, A., Han, Z.-Y., Votzke, S., Yammine, A., & Gibert, J. P. (2021). Linking species traits and demography to explain complex temperature responses across levels of organization. *Proceedings of the National Academy of Sciences*, *118*(42), e2104863118. https://doi.org/10.1073/pnas.2104863118

803 Wieczynski, D. J., Yoshimura, K. M., Denison, E. R., Geisen, S., DeBruyn, J. M., Shaw, A. J., Weston,
804 D. J., Pelletier, D. A., Wilhelm, S. W., & Gibert, J. P. (2023). Viral infections likely mediate
805 microbial controls on ecosystem responses to global warming. *FEMS Microbiology Ecology*,
806 *99*(3), fiad016. https://doi.org/10.1093/femsec/fiad016
807 Winey, M., Stemm-Wolf, A. J., Giddings, T. H., & Pearson, C. G. (2012). Cytological analysis of
808 Tetrahymena thermophila. *Methods in Cell Biology*, *109*, 357–378. https://doi.org/10.1016/B978-
809 0-12-385967-9.00013-X
810 Xiong, W., Song, Y., Yang, K., Gu, Y., Wei, Z., Kowalchuk, G. A., Xu, Y., Jousset, A., Shen, Q., &
811 Geisen, S. (2020). Rhizosphere protists are key determinants of plant health. *Microbiome*, *8*(1),
812 27. https://doi.org/10.1186/s40168-020-00799-9
813 Xu, M., & Shang, H. (2016). Contribution of soil respiration to the global carbon equation. *Journal of*
814 *Plant Physiology*, *203*, 16–28. https://doi.org/10.1016/j.jplph.2016.08.007
815 Zufall, R. A., Dimond, K. L., & Doerder, F. P. (2013). Restricted distribution and limited gene flow in the
816 model ciliate Tetrahymena thermophila. *Molecular Ecology*, *22*(4), 1081–1091.
817 https://doi.org/10.1111/mec.12066

Online Supplementary Materials: Temperature-dependent selection shapes microbial thermal performance curves and population genetic makeup

Megan H. Liu[1], Ze-Yi Han[1], Yaning Yuan[1], Katrina DeWitt[1], Daniel J. Wieczynski[1], Kathryn M. Yammine[2], Andrea Yammine[1], Rebecca Zufall[3], Adam Siepielski[4], Douglas Chalker[5], Masayuki Onishi[1], Fabio A. Machado[6], Jean P. Gibert[1]

[1]Department of Biology, Duke University, Durham, NC, 27708, USA
[2]Department of Chemistry, Massachusetts Institute of Technology, Cambridge, MA, 02139, USA
[3]Department of Biology and Biochemistry, University of Houston, Houston, TX 77204, USA
[4]Department of Biological Sciences, University of Arkansas, Fayetteville, AR, USA
[5]Department of Biology, Washington University, Saint Louis, MI, USA
[6]Department of Integrative Biology, Oklahoma State University, Stillwater, OK, USA

INDEX:

Appendix S1. r_peak Stats Table

	Estimate	SD	P-value
Linear term	1.81	0.16	**≤0.001**
Quadratic term	-0.28	0.12	0.24
Low Temp	-6.25	0.26	**≤0.001**
Med Temp	-3.20	0.26	**≤0.001**
Linear*LowTemp	-2.13	0.22	**≤0.001**
Linear*MedTemp	-1.27	0.22	**≤0.001**
Quadratic*LowTemp	0.14	0.17	0.70
Quadratic*MedTemp	-0.08	0.17	0.82

Appendix S2. E_a Stats Table

	Estimate	SD	P-value
Linear term	1.61	0.15	**≤0.001**
Quadratic term	-0.12	0.13	0.62
Low Temp	-6.07	0.27	**≤0.001**
Med Temp	-3.06	0.27	**≤0.001**
Linear:LowTemp	-2.03	0.21	**≤0.001**
Linear:MedTemp	-1.20	0.21	**≤0.001**
Quadratic:LowTemp	-0.22	0.18	0.53
Quadratic:MedTemp	-0.34	0.18	0.33

Appendix S3. CT_min Stats Table

	Estimate	SD	P-value
Linear term	0.44	0.18	**0.02**
Quadratic term	-0.12	0.13	0.66
Low Temp	-6.15	0.32	**≤0.001**
Med Temp	-3.21	0.32	**≤0.001**
Linear*LowTemp	-1.19	0.26	**≤0.001**
Linear*MedTemp	-0.88	0.26	**≤0.001**
Quadratic*LowTemp	-0.04	0.19	0.90
Quadratic*MedTemp	-0.06	0.19	0.89

Appendix S4. T_opt Stats Table

	Estimate	SD	P-value
Linear term	-0.32	0.20	0.11
Quadratic term	-2.10	0.21	**≤0.001**
Low Temp	-7.43	0.40	**≤0.001**
Med Temp	-3.95	0.40	**≤0.001**
Linear*LowTemp	0.01	0.28	0.98
Linear*MedTemp	-0.23	0.28	0.42
Quadratic*LowTemp	2.52	0.30	**≤0.001**
Quadratic*MedTemp	1.42	0.30	**0.02**

Appendix S5. Genotype Table

Name	Original Provenance	Provenance	Stock ID	Mutations
20395-1	Lake Warren in Alstead, NH, lat. 43 07.310, long. -72 17.840	Cornell Tetrahymena Stock Center	SD01557	NA
SB3539-I		Cornell Tetrahymena Stock Center	SD00660	*chx1[C3]-1/chx1[C3]-1 (CHX1[C3]; cy-s, I)*, C3 strain - functional heterokaryon carrying cycloheximide resistance in micronucleus.
B*VII		Cornell Tetrahymena Stock Center	SD00023	B strain star line. Lacks a genetically functional micronucleus.
B2192 III	Frankel lab (Leslie Jenkins)	Cornell Tetrahymena Stock Center	SD01754	Derived from a cross of B2086 II x B2086 VIa. Isogenic with B2192 IVB
CU428.2		Cornell Tetrahymena Stock Center	SD00178	*mpr1-1/mpr1-1* (*MPR1*; mp-s, VII)
DMCK72H	Chalker Lab, Washington University in St. Louis			
19877	SG69-4 in Guys Mills, PA (lat. 41 38.023, long. -79 53.514, elevation 1660 ft)	Cornell Tetrahymena Stock Center	SD01555	Cech's self-splicing intron is present. Cytochrome oxidase I haplotype = WPA1
19617-1	FS136E in PA (latitude 41.46, longitude -78.88)	Cornell Tetrahymena Stock Center	SD03089	

IMB6 (GFP)	Chalker Lab, Washington University in St. Louis			
A*V		Cornell Tetrahymena Stock Center	SD00014	Lacks a genetically functional micronucleus.
20441-1	Gregg Lake in Antrim, NH (lat. 43 02.605, long. -71 59.383	Cornell Tetrahymena Stock Center	SD01560	
CU427-4		Cornell Tetrahymena Stock Center	SD00715	chx1-1/chx1-1 (CHX1; cy-s, VI)
SB1518		Cornell Tetrahymena Stock Center	SD01537	*gal1-1/gal1-1; tyr-14/tyr-14*
IA388		Cornell Tetrahymena Stock Center	SD01454	*elo1-1/elo1-1* (*elo1*; II)
21157-1	FS343S in PA (latitude 41.45, longitude -78.88)	Cornell Tetrahymena Stock Center	SD03114	
CU438-1		Cornell Tetrahymena Stock Center	SD00189	*pmr1-1/pmr1-1*
CU304		Cornell Tetrahymena Stock Center	SD00051	CHX1/CHX1; chx2-1/chx2-1; mpr1-1/mpr1-1
CU4106		Cornell Tetrahymena Stock Center	SD01010	*mpr1-1/mpr1-1*
AXS	Chalker Lab, Washington University in St. Louis			
C*III		Cornell Tetrahymena Stock Center	SD00024	C strain star line. Lacks a genetically functional micronucleus.

Appendix S6. Flow Cytometry Frequency Calculations

Each microcosm was censused with a Novocyte 2000R flow cytometer and analyzed using NovoExpress software v15.0. The flow cytometer detects particles (e.g., cells, debris, bacteria) based on how they scatter light and fluoresce [1]. Light scattering properties can be used to quantify cell size (FSC-H), and we detected fluorescence in the Phycoerythrin (PE-H, yellow) and Fluorescein isothiocyanate (FITC-H) channels. We gated the data in NovoExpress to select for the largest particles which in our case were all *Tetrahymena thermophila* cells. The data are plotted in Fig 8.1. We used a PE-H versus FITC-H plot to parse the different fluorescent signals between the two experimental strains: CU4106 (which autofluoresces exclusively) and AXS (which autofluoresces and expresses Yellow Fluorescent Protein, or YFP). Control microcosms, which contained exclusively one of either strain for each temperature treatment, were used to determine the exact expected fluorescence range for each individual cell. An "AutoF" and "YFP" gate were created based on these controls (Figure 1). These control gating filters were then applied over each experimental microcosm, allowing us to identify cell strain based on their fluorescence pattern.

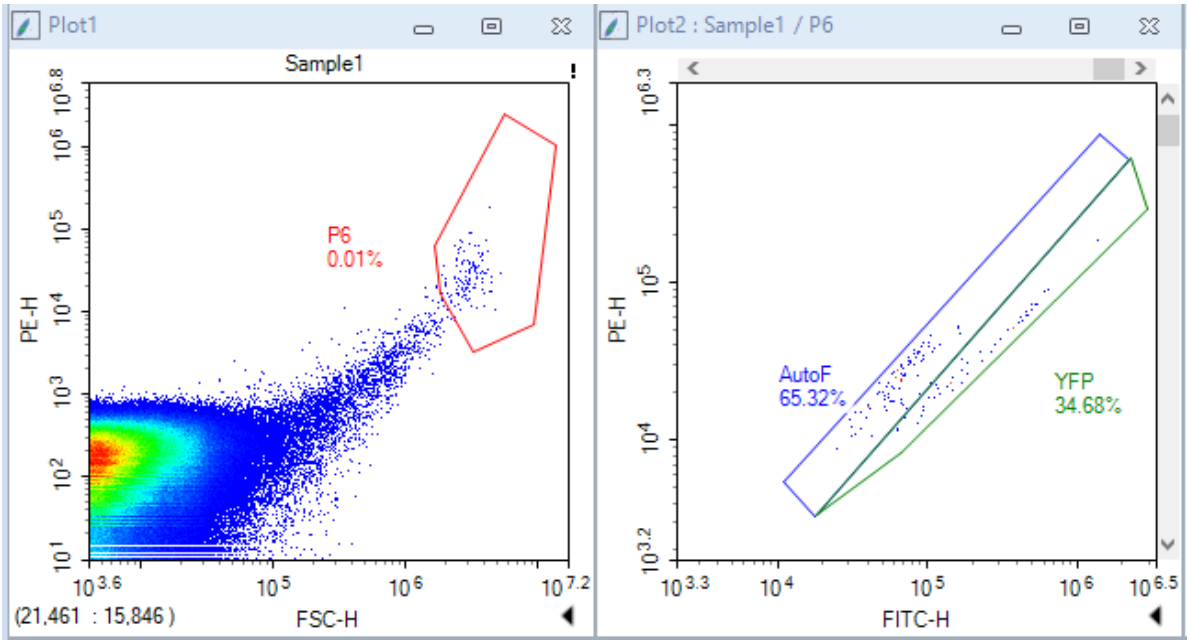

Appendix S6 Figure 1. This plot shows an AXS control sample, where 65% of AXS individuals fluoresced in the autofluorescence gating range.

We used two CU4106 control microcosms and nine AXS control microcosms per temperature. Additional AXS controls were necessary to increase detection precision while gating. Non-YFP tagged cells (CU-4106) fluoresced more weakly in the FITC-H channel than YFP-tagged cells (AXS) and generally fluoresced more strongly in the PE-H channel than non-YPF tagged cells fluorescence. CU4106 controls were detected exclusively in the autofluorescent gate. However, AXS controls were detected in both the autofluorescent ("AutoF") and YFP gates, meaning that we could expect AXS cells to show up in the AutoF gate under experimental conditions, thus making it harder to parse YFP-tagged from non-YFP tagged cells.

To resolve that, we thus used the control microcosms to adjust the relative frequencies of each strain in each experimental microcosm, calculated as follows. For each single-strain control microcosm, we calculated the proportion of cells detected in each of the two gates across temperatures (Table X). We then used the proportion of AXS cells across control replicates to adjust the observed number of AXS cells (i.e., cells showing up on the YFP gate) to ensure our estimate was as accurate as possible. We then subtracted this adjusted count from the total number of individuals in each microcosm to generate our final adjusted experimental count of CU4106 individuals. See Appendix Table 10 below for pertinent data.

Appendix S7. Table of Frequency Calculations

	temp	rep	AB +/-	proportion	CU4106 count	adjusted CU4106 count	AXS count	adjusted AXS count	total
1	19	Sample1	NoAB	0.51421189	5	5.000000	0	0.000000	5
2	19	Sample2	AB	0.01271186	71	71.000000	0	0.000000	71
3	19	Sample2	NoAB	0.51421189	20	18.110553	2	3.889447	22
4	19	Sample3	NoAB	0.51421189	37	34.165829	3	5.834171	40
5	19	Sample4	AB	0.01271186	53	53.000000	0	0.000000	53
6	19	Sample4	NoAB	0.51421189	17	17.000000	0	0.000000	17
7	19	Sample6	AB	0.01271186	49	49.000000	0	0.000000	49
8	19	Sample6	NoAB	0.51421189	9	8.055276	1	1.944724	10
9	19	Sample7	AB	0.01271186	76	76.000000	0	0.000000	76
10	19	Sample7	NoAB	0.51421189	32	32.000000	0	0.000000	32
11	22	Sample1	AB	0.58564815	73	72.292490	1	1.707510	74
12	22	Sample1	NoAB	0.40142857	105	99.035587	4	9.964413	109
13	22	Sample2	AB	0.58564815	77	74.877470	3	5.122530	80
14	22	Sample2	NoAB	0.40142857	34	11.633452	15	37.366548	49
15	22	Sample3	AB	0.58564815	12	9.877470	3	5.122530	15
16	22	Sample3	NoAB	0.40142857	37	32.526690	3	7.473310	40
17	22	Sample4	AB	0.58564815	22	2.897233	27	46.102767	49
18	22	Sample6	AB	0.58564815	13	12.292490	1	1.707510	14
19	22	Sample6	NoAB	0.40142857	13	11.508897	1	2.491103	14
20	22	Sample7	AB	0.58564815	7	6.292490	1	1.707510	8
21	22	Sample7	NoAB	0.40142857	21	21.000000	0	0.000000	21
22	25	Sample1	AB	0.27131609	162	33.084581	48	176.915419	210
23	25	Sample1	NoAB	0.55903491	254	129.370065	158	282.629935	412
24	25	Sample2	AB	0.27131609	358	113.597851	91	335.402149	449

25	25	Sample2	NoAB	0.55903491	179	73.301194	134	239.698806	313
26	25	Sample3	AB	0.27131609	309	169.341629	52	191.658371	361
27	25	Sample3	NoAB	0.55903491	192	104.443526	111	198.556474	303
28	25	Sample4	AB	0.27131609	246	165.427863	30	110.572137	276
29	25	Sample4	NoAB	0.55903491	261	212.094582	62	110.905418	323
30	25	Sample5	AB	0.27131609	263	220.028194	16	58.971806	279
31	25	Sample5	NoAB	0.55903491	180	169.745638	13	23.254362	193
32	25	Sample6	AB	0.27131609	597	438.541464	59	217.458536	656
33	25	Sample6	NoAB	0.55903491	193	127.529844	83	148.470156	276
34	25	Sample7	AB	0.27131609	291	145.970153	54	199.029847	345
35	25	Sample7	NoAB	0.55903491	184	137.460974	59	105.539026	243
36	30	Sample1	AB	0.13819840	1445	902.470286	87	629.529714	1532
37	30	Sample1	NoAB	0.44750154	263	235.838158	22	49.161842	285
38	30	Sample2	AB	0.13819840	732	588.572604	23	166.427396	755
39	30	Sample2	NoAB	0.44750154	244	202.022608	34	75.977392	278
40	30	Sample3	AB	0.13819840	1566	1191.841576	60	434.158424	1626
41	30	Sample3	NoAB	0.44750154	460	399.503170	49	109.496830	509
42	30	Sample4	AB	0.13819840	848	93.447179	121	875.552821	969
43	30	Sample4	NoAB	0.44750154	341	249.637440	74	165.362560	415
44	30	Sample5	AB	0.13819840	328	128.448841	32	231.551159	360
45	30	Sample5	NoAB	0.44750154	372	307.799282	52	116.200718	424
46	30	Sample6	NoAB	0.44750154	354	287.330024	54	120.669976	408
47	30	Sample7	AB	0.13819840	1908	1459.009892	72	520.990108	1980
48	30	Sample7	NoAB	0.44750154	233	209.542045	19	42.457955	252
49	32	Sample1	AB	0.21434368	536	169.459535	100	466.540465	636
50	32	Sample1	NoAB	0.28314509	161	90.110769	28	98.889231	189
51	32	Sample2	AB	0.21434368	580	492.030288	24	111.969712	604

52	32	Sample2	NoAB	0.28314509	215	171.960110	17	60.039890	232
53	32	Sample3	AB	0.21434368	578	515.688121	17	79.311879	595
54	32	Sample3	NoAB	0.28314509	252	219.087143	13	45.912857	265
55	32	Sample4	AB	0.21434368	2101	1873.744911	62	289.255089	2163
56	32	Sample4	NoAB	0.28314509	121	77.960110	17	60.039890	138
57	32	Sample5	AB	0.21434368	550	201.786558	95	443.213442	645
58	32	Sample5	NoAB	0.28314509	109	60.896593	19	67.103407	128
59	32	Sample6	AB	0.21434368	473	418.018930	15	69.981070	488
60	32	Sample6	NoAB	0.28314509	259	183.047253	30	105.952747	289
61	32	Sample7	AB	0.21434368	2796	1890.645050	247	1152.354950	3043
62	32	Sample7	NoAB	0.28314509	201	157.960110	17	60.039890	218
63	38	Sample2	AB	0.07118688	1135	273.862817	66	927.137183	1201
64	38	Sample2	NoAB	0.07573333	795	380.056343	34	448.943657	829
65	38	Sample3	AB	0.07118688	1051	385.575813	51	716.424187	1102
66	38	Sample3	NoAB	0.07573333	1912	264.429596	135	1782.570404	2047
67	38	Sample4	AB	0.07118688	5506	3209.634179	176	2472.365821	5682
68	38	Sample4	NoAB	0.07573333	1146	718.852117	35	462.147883	1181
69	38	Sample5	AB	0.07118688	537	484.809868	4	56.190132	541
70	38	Sample5	NoAB	0.07573333	710	295.056343	34	448.943657	744
71	38	Sample6	AB	0.07118688	1323	1179.477136	11	154.522864	1334
72	38	Sample6	NoAB	0.07573333	1307	1111.732397	16	211.267603	1323
73	38	Sample7	AB	0.07118688	1160	886.001805	21	294.998195	1181
74	38	Sample7	NoAB	0.07573333	959	324.380289	52	686.619711	1011

Appendix S8. Alternative Experimental Conditions With and Without Antibiotics

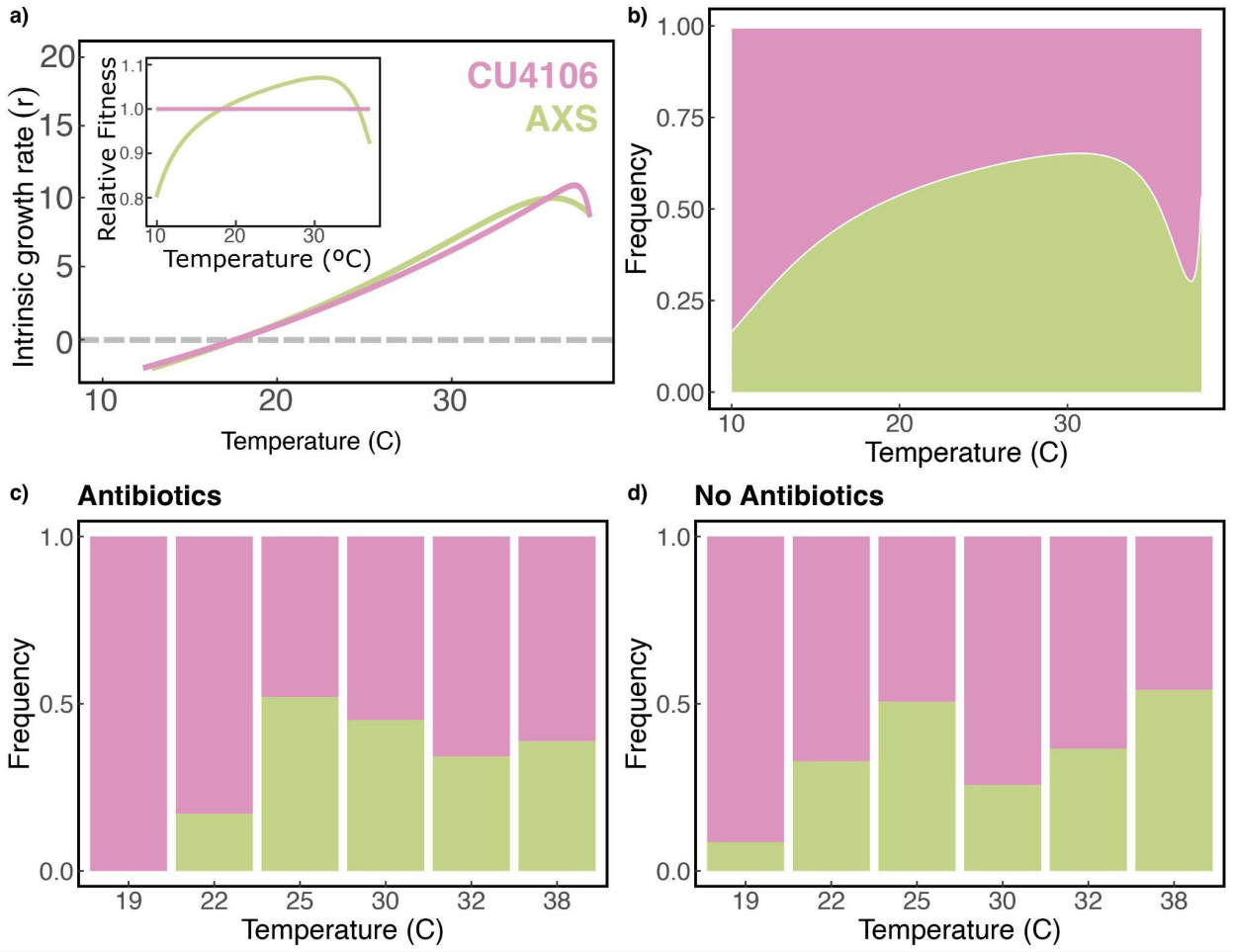

Fig Appendix S8: a) r-TPC for genotypes CU4106 and AXS. Inset: Measures of relative fitness for both CU4106 and AXS. This predicts an increase in AXS frequency relative to CU4106 at intermediate temperatures relative to low or high temperatures. b) Predicted genetic frequencies across temperatures. c) Observed genetic frequencies across temperatures with Paromomycin. d) As in c) but without Paromomycin.

Appendix S9. Differential Fluorescence Across Strains

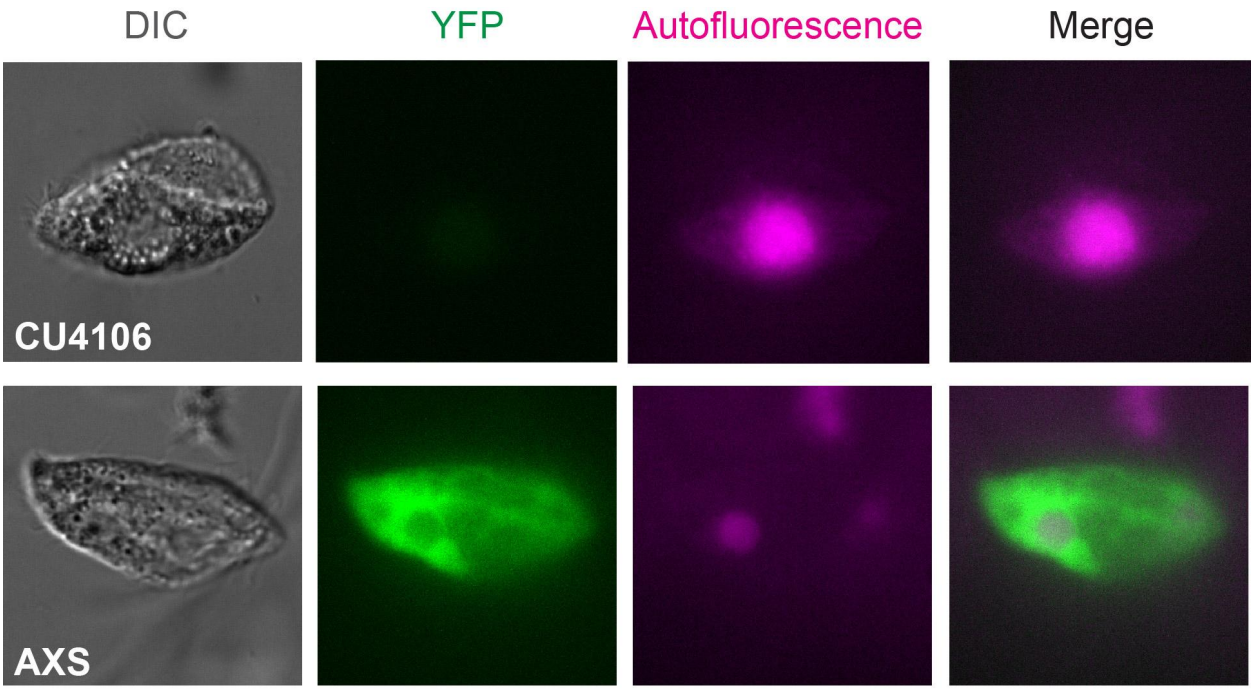

1st column: Differential Interference Contrast (DIC) microscopy for CU4016 and AXS protist Tetrahymena thermophila (CU4106 and AXS). Subsequent columns display raw fluorescence microscopy images. Photos are unimposed and uncorrected for relative fluorescence levels.

REFERENCES

1. McKinnon, K. M. Flow Cytometry: An Overview. *Curr. Protoc. Immunol.* **120**, 5.1.1-5.1.11 (2018).